

# Mid-infrared quantum cascade laser based off-axis integrated cavity output spectroscopy for biogenic nitric oxide detection

Yury A. Bakhrkin, Anatoliy A. Kosterev, Chad Roller, Robert F. Curl, and Frank K. Tittel

Tunable-laser absorption spectroscopy in the mid-IR spectral region is a sensitive analytical technique for trace-gas quantification. The detection of nitric oxide (NO) in exhaled breath is of particular interest in the diagnosis of lower-airway inflammation associated with a number of lung diseases and illnesses. A gas analyzer based on a continuous-wave mid-IR quantum cascade laser operating at  $\sim 5.2 \mu\text{m}$  and on off-axis integrated cavity output spectroscopy (ICOS) has been developed to measure NO concentrations in human breath. A compact sample cell, 5.3 cm in length and with a volume of  $< 80 \text{ cm}^3$ , that is suitable for on-line and off-line measurements during a single breath cycle, has been designed and tested. A noise-equivalent (signal-to-noise ratio of 1) sensitivity of 10 parts in  $10^9$  by volume (ppbv) of NO was achieved. The combination of ICOS with wavelength modulation resulted in a 2-ppbv noise-equivalent sensitivity. The total data acquisition and averaging time was 15 s in both cases. The feasibility of detecting NO in expired human breath as a potential noninvasive medical diagnostic tool is discussed.

© 2004 Optical Society of America

OCIS codes: 280.3420, 300.6340, 140.5960, 170.4580, 000.1430.

## 1. Introduction

Nitric oxide (NO) detection is important for a number of applications such as atmospheric pollution monitoring,<sup>1</sup> vehicle exhaust control,<sup>2,3</sup> and noninvasive medical diagnostics of various lung diseases by means of NO concentration measurements in expired breath.<sup>4,5</sup> In fact, exhaled breath contains a large number of molecular species at ultralow concentrations [parts in  $10^9$  by volume (ppbv)], some of which are possible biomarkers for a variety of human illnesses and diseases. Trace-gas quantification in breath is inherently noninvasive and in some cases can obviate the need for invasive surgical procedures such as biopsies.

NO is involved in many biochemical processes and performs important functions in human physiology

such as immune reactions, neurotransmission, and regulation of platelet function.<sup>6–13</sup> In 1998 the Nobel Prize in Physiology and Medicine recognized discoveries concerning the role of NO in the cardiovascular system.

Concentrations of oral exhaled nitric oxide (eNO) that originates from the lower airways in the absence of asthma and acute respiratory illnesses typically vary from 5 to 20 ppbv.<sup>9,10</sup> Nasal nitric oxide (nNO) that originates from the nasal cavity has higher concentrations, ranging from 40 to 200 ppbv.<sup>9,10</sup> Humming, a voice maneuver, has been reported to produce 200 to 500 ppbv of NO in expired breath.<sup>6,8</sup>

Concentrations of eNO are reduced below typical levels in patients with cystic fibrosis<sup>12</sup> and in smokers.<sup>13</sup> Elevated eNO concentrations in expired breath are associated principally with inflammation of the lower airways. Asthma is one of the most investigated inflammatory disorders. Asthma is a chronic inflammatory disorder of the lower airways that results in increased levels of eNO in human exhaled air.<sup>9</sup> Noninvasive diagnostics of asthma, which afflicts millions of adults and children worldwide, are of great importance, and early diagnosis and intervention in asthma cases can lead to a significant reduction in the number of

---

The authors are with the Department of Electrical and Computer Engineering, Rice University, 6100 South Main Street, Houston, Texas 77005-1892. F. K. Tittel's e-mail address is fkt@rice.edu.

Received 22 October 2003; revised manuscript received 5 January 2004; accepted 22 January 2004.

0003-6935/04/112257-10\$15.00/0

© 2004 Optical Society of America

patient hospitalizations. Typical asthmatic eNO levels in exhaled breath range from 20 to 80 ppbv.<sup>9,10</sup> Therefore NO detection and quantification at the level of parts in  $10^9$  by volume in human exhalation poses an important medical diagnostic challenge.<sup>10</sup>

A number of different analytical methods, both optical and nonoptical, have been developed to measure ultralow concentrations of various gases, particularly NO. Nonoptical approaches include mass spectrometry and gas chromatography. The main drawbacks of these techniques are the size and cost of the apparatus, the need for sample conditioning and consumables, and the inability to make real-time on-line measurements. The most advanced optical techniques are based on either chemiluminescence or laser absorption spectroscopy. Chemiluminescence is widely used for measuring eNO levels in both children and adults. This technique has been approved by the U.S. Food and Drug Administration and has a minimum detection sensitivity of  $<1$  ppbv.<sup>11</sup> Two companies, Sievers and more recently Aerocrine, have developed analyzers based on a chemiluminescence approach for high-precision real-time NO monitoring. This technique requires calibration at the same humidity and temperature as breath and can also measure NO<sub>2</sub>. Another optical method for precise NO measurements is based on the Zeeman and Faraday effects and makes use of the paramagnetic properties of NO. Background-free Faraday laser magnetic resonance spectroscopy (Faraday-LMRS) measures only NO in human breath.<sup>8,14,15</sup> The method was evaluated in a clinical environment for on-line NO monitoring with a detection sensitivity of  $\sim 1$  ppbv.<sup>8</sup> However, because Faraday-LMRS requires a magnetic field of more than 1000 Gauss and is incapable of measuring nonparamagnetic gases, its applicability to clinical diagnostics is limited. An ideal eNO sensor platform should be able to measure other gases (e.g., CO and CO<sub>2</sub>) in exhaled breath for calibration and standardization purposes.<sup>16</sup>

In this work we investigate tunable-laser absorption spectroscopy (TLAS) as an effective technique for sensitive and selective NO monitoring. The mid-IR spectral range is ideally suited for TLAS because most molecular gases possess strong fundamental rotational-vibrational lines in this region. The NO molecule has a strong absorption band near  $5.2 \mu\text{m}$  ( $1900 \text{ cm}^{-1}$ ) with a highest line intensity of  $\sim 6.04 \times 10^{-20} \text{ cm}^{-1}/(\text{molecule cm}^{-2})$  for the  $R(7.5)$  NO lines at  $1903.1 \text{ cm}^{-1}$ . High-resolution TLAS with a tunable single-frequency mid-IR laser can resolve NO absorption features and selectively access NO spectral lines at low ( $\leq 100$  Torr) pressure without interference from CO<sub>2</sub> and H<sub>2</sub>O. This is particularly important in the development of biomedical gas sensors for breath analysis. Several types of continuous-wave (cw) spectroscopic laser sources operate in the mid-IR spectral region. These include the optical parametric oscillator, coherent sources based on difference frequency generation,

lead-salt diode lasers, and quantum cascade (QC) lasers. QC lasers were selected for this work on account of their potential to meet the spectroscopic source requirements for compact, sensitive, and selective gas detectors.<sup>17</sup> Two cw distributed-feedback QC lasers were utilized in our sensor architecture (as described in Section 2). Each of these lasers has a spectral width of  $\approx 3.0$  MHz, and together they provide a total single-mode tuning range of  $>10 \text{ cm}^{-1}$ .

To obtain detection sensitivities at levels of parts in  $10^9$  by volume or lower, long optical path lengths ( $\geq 30$  m), usually realized in multipass absorption cells, are used.<sup>16,18-20</sup> As can be deduced from the results presented in Ref. 20, a sensitivity of  $0.7 \text{ ppb}/\text{Hz}^{1/2}$  can be achieved by use of a multipass cell with a 36-m path and a 0.3-L volume (Aerodyne Research, Inc., Model AMAC 36). Another approach for achieving long optical path length and minimizing gas-cell volumes is to use a cavity that consists of two ultralow-loss dielectric mirrors [ $\sim 100$  parts in  $10^6$  (ppm)] separated by a few centimeters. In this manner, effective optical path lengths of hundreds of meters can be realized. Absorption in the cavity can be measured from the change in the cavity ringdown time or from the time-integrated cavity output. The first method, known as cavity ringdown spectroscopy (CRDS), has been successfully applied to measure NO concentrations at parts in  $10^9$  by volume levels.<sup>17,21</sup> The second approach for measuring absorption in the cavity is based on the excitation of a dense spectrum of transverse cavity modes and time averaging of the cavity output. In this scheme the greater the number of modes that are excited, the easier it is to suppress the related cavity throughput fluctuations. This method was first reported by two groups almost simultaneously and is referred to as integrated cavity output spectroscopy (ICOS) or cavity enhanced absorption spectroscopy.<sup>22,23</sup> ICOS is less technically demanding than CRDS because it does not require fast time-resolved measurements, high laser-pulse energies, or narrow cw laser linewidths. ICOS with an on-axis laser-cavity configuration has been used to measure NO with a detection limit of 16 ppbv.<sup>19</sup> Off-axis ICOS (OA-ICOS) was proposed and implemented in near-IR because it provides increased spectral density of cavity modes and thus minimizes the noise in the resulting absorption spectra.<sup>24-26</sup> In OA-ICOS the laser beam is directed at an angle with respect to the cavity axis. In this paper we describe the use of the OA-ICOS technique with a cw mid-IR QC laser to measure NO concentrations in a compact absorption cell ( $76 \text{ cm}^3$ ). A NO analyzer with a noise-equivalent [signal-to-noise ratio (SNR) of 1] sensitivity of 10 ppbv for OA-ICOS alone and 2 ppbv for OA-ICOS with wavelength modulation was demonstrated and used to detect NO in a nasal breath sample. The time required to obtain the reported sensitivity was 15 s in both cases.

## 2. Off-Axis Integrated Cavity Output Spectroscopy Technique

The off-axis laser-cavity geometry has several advantages over CRDS or a multipass cell direct absorption approach:

- No need for submicrosecond time-resolved measurements;
- Low requirements for cavity mode stability and hence mechanical stability;
- Simplified alignment; and
- Small cell volume.

A high-order transverse cavity TEM<sub>*mn*</sub> mode has (*n* + *m*) times smaller free spectral range (FSR) compared with TEM<sub>00</sub> mode. Off-axis alignment causes an excitation of many transverse modes of different orders. This results in a more efficient averaging of the cavity output and an order of magnitude improvement in detection sensitivity through reduced noise. The resulting compact cell design is compatible with the requirements for a portable clinical sensor. For quantitative concentration measurements, OA-ICOS requires that the sensor be calibrated after each realignment of the OA-ICOS cell.

A compact cell is required for our specific application of NO detection in breath. Because NO is a chemically active gas, concentration measurements should be carried out in flowing gas. It is also desirable to obtain the concentration profile during a single breath cycle to derive the NO production from different parts of the airway. Because the typical breath volume is ~500 cm<sup>3</sup> and a breath cycle is ~4 s, the cavity volume should be between 10 and 100 cm<sup>3</sup>, and the data acquisition time <1 s. A critical design issue for the OA-ICOS breath analyzer configuration is the use of cavity mirrors with a diameter large enough to allow multiple reflections of the laser beam inside the cavity without causing beam overlaps on the mirror surfaces. This decreases the fringe contrast and provides a higher SNR. Therefore a pair of 50.8-mm diameter mirrors (radius of curvature of 1 m, *R* = 99.975; Los Gatos Research, Inc., Mountain View, Calif.) was selected. To maintain the required small cell volume, the mirrors were positioned 5.3 cm apart.

Off-axis beam propagation in a stable two-mirror cavity was first analyzed by Herriott, Kogelnik, and Kompfner.<sup>27</sup> The cavity used here satisfies the following stability condition:

$$0 < (1 - L/r)^2 < 1, \quad (1)$$

where *L* is the mirror spacing (cavity length) and *r* = *r*<sub>1</sub> = *r*<sub>2</sub> is the radius of mirror curvature (i.e., the cavity is formed by two identical spherical mirrors). The previous analysis<sup>27</sup> demonstrates that the spot pattern on the mirrors generally lies on an ellipse. To maximize the circumference that can be fitted onto the mirror surface and thus the number of spots that can be accommodated without overlap, the elliptical form should be a circle near the edge of the mirrors,

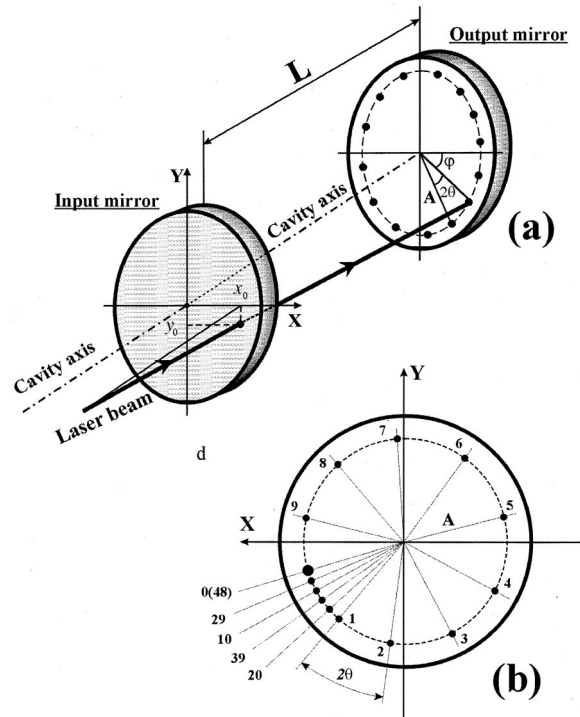


Fig. 1. (a) Off-axis beam propagation. *L* is the cavity length (5.3 cm in our experiments); *x*<sub>0</sub>, *y*<sub>0</sub>, the coordinates of the injected laser beam on the input mirror. (b) Laser spots on the input mirror. Numbers corresponding to spots reflect the numbers of round-trip passes within the cavity. The reentrant condition occurs after 48 round-trip passes. *A* is the radius of the circle of laser spots.

as shown in Fig. 1(a). Herriott *et al.* calculated the initial beam direction required to form a circle. Because the orientation of an *X*, *Y* axis system on the mirror is arbitrary, one (*x*<sub>0</sub>') of the four variables, *x*<sub>0</sub>, *y*<sub>0</sub>, *x*<sub>0</sub>', *y*<sub>0</sub>' (where *x*<sub>0</sub>, *y*<sub>0</sub> determine the location of the spot and *x*<sub>0</sub>', *y*<sub>0</sub>' determine the ray's direction) can be set equal to zero and then the requirement that the spots lie on a circle of radius *A* determines the other three parameters. The initial slope, *y*<sub>0</sub>', is given by

$$y_0' = A/\sqrt{fL}, \quad (2)$$

where *f* = *r*/2 (focal length of the mirror). Somewhat surprisingly, the angle 2θ of a round-trip rotation of the beam spot is determined solely by the mirror spacing and curvature:

$$\cos \theta = 1 - L/r. \quad (3)$$

The reentrant condition is satisfied if

$$2m\theta = 2n\pi, \quad (4)$$

where *m* is the number of the beam round trips, *n* is an integer, and after every *m* round trips the ray starts to retrace its path [see Fig. 1(b)]. The FSR of such a cavity mode is *c*/(2*Lm*). From Eqs. (3) and (4), *m* is determined only by the geometrical parameters of the cavity and not by the beam alignment. For OA-ICOS it is desirable to have the highest possible value of *m* that can be achieved without having

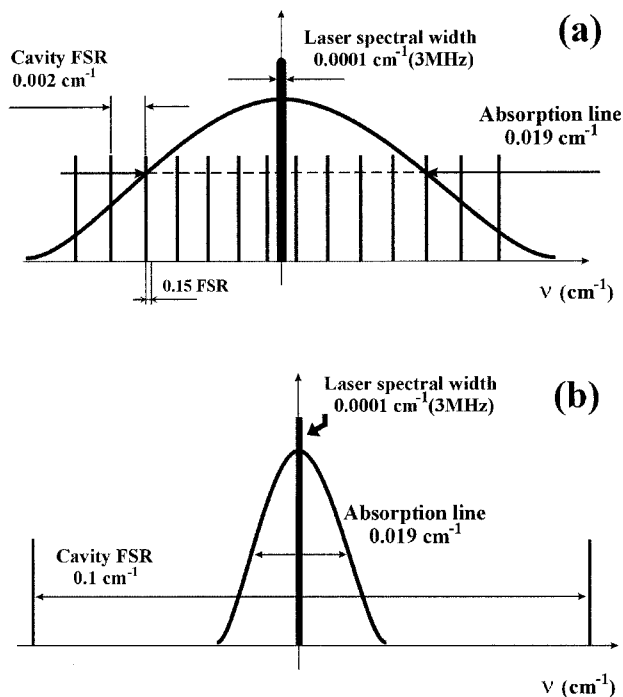


Fig. 2. (a) Frequency hierarchy for off-axis alignment when the reentrant condition is satisfied after 48 round trips. Spectral width of the cavity mode is 0.2 MHz. Fluctuations of the cavity FSR due to thermal displacement of the mirrors are of the order of 0.15 FSR. (b) The same hierarchy for on-axis laser-cavity alignment. Spectral width of the absorption line is  $0.019 \text{ cm}^{-1}$ , laser linewidth  $\sim 1 \times 10^{-4} \text{ cm}^{-1}$  ( $\sim 3 \text{ MHz}$ ), cavity FRS =  $0.1 \text{ cm}^{-1}$ .

overlapping beams. Therefore mirror spacing should be chosen so as to avoid low- $m$  conditions. For example, a confocal resonator satisfies the reentrant condition for  $m = 2$ .

In our design the cavity length is 5.3 cm and the mirror radius of curvature is 100 cm. According to relations (3) and (4),  $m = 48$ ,  $n = 5$ , and  $\text{FSR} = 0.002 \text{ cm}^{-1}$  [59 MHz; see Fig. 2(a)]. The cavity length was intentionally detuned from 5 cm, where the reentrant condition is satisfied after only 10 round-trip passes.

We believe that the choices made here are optimum for spherical mirrors. Astigmatic optics can significantly extend the optical path before satisfying the reentrant condition and can improve the off-axis performance of a compact cell, because the spot patterns lie on Lissajous curves for astigmatic mirrors.<sup>24</sup> This allows use of more of the mirror surface. However, high-quality astigmatic mirrors are difficult to fabricate.

The ideal case for ICOS is achieved when the effective cavity FSR is significantly smaller than the laser linewidth. Once this condition is satisfied, the resonant cavity properties disappear and the cavity output does not depend on laser frequency over a narrow range, effectively eliminating the noise caused by the transmission variations as the laser scans from mode to mode. However, in practice, it is difficult to make the FSR small enough for a short cell and a narrow laser bandwidth. Instead, to reduce

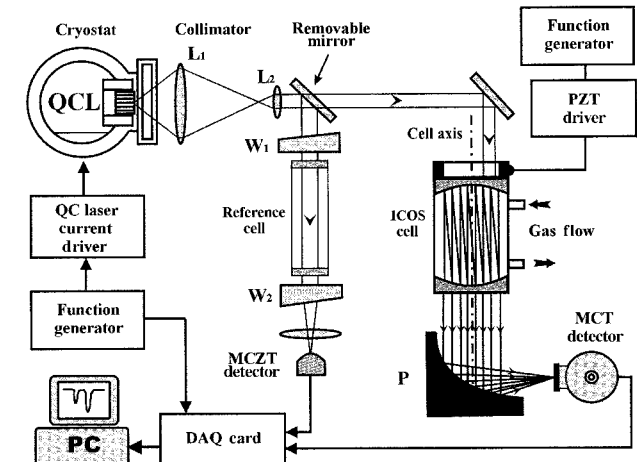


Fig. 3. Off-axis ICOS experimental arrangement:  $L_1$  and  $L_2$ , two collimating lenses;  $W_1$  and  $W_2$ , two 30' wedged uncoated ZnSe windows for frequency calibration; QCL, the QC laser mounted inside a cryostat; P, an off-axis parabolic mirror; MCZT, a room-temperature HgCdZnTe photodetector.

the fringe contrast, which introduces noise, the laser frequency can be rapidly scanned through the cavity mode and/or one of the cavity mirrors can be dithered to generate random jittering of the cavity modes. In this work we combined these methods. A mirror displacement with a piezoelectric actuator results in a better SNR under the same averaging conditions, yielding improved sensitivity.

Because the high mirror reflectivity permits the introduction of only a small fraction of invisible laser radiation, it is difficult to monitor the laser spot patterns. Instead, a convenient method of alignment is to monitor the SNR of the cavity output.

### 3. Experimental Arrangement

The experimental arrangement is shown in Fig. 3. The laser source utilized in the experiments is a cw distributed-feedback QC laser (Lucent Technologies Inc., Murray Hill, N.J.) operating at a single frequency at liquid-nitrogen ( $\text{LN}_2$ ) temperature.<sup>28</sup> A laser chip containing several QC lasers with output at  $\sim 5.2 \mu\text{m}$  ( $\sim 1920 \text{ cm}^{-1}$ ) is mounted on a cold finger inside a  $\text{LN}_2$  cryostat with one laser selected for usage. For better beam stability, a special design of the  $\text{LN}_2$  cryostat (Model DET-1746-SLN from Cryo Industries, Manchester, N.H.) was used. The cryostat has a rigid support for the  $\text{LN}_2$  reservoir, preventing mechanical displacement of the cold finger and thus the QC laser during the cryostat refilling process and the entire  $\text{LN}_2$  holding period. A current driver (MPL-5000, Wavelength Electronics, Bozeman, Mont.) is used to operate the QC lasers. A current ramp with a maximum frequency of 5 kHz was applied to tune the laser frequency. In this work we used two QC lasers: one with a tuning range of  $1911.5\text{--}1917.5 \text{ cm}^{-1}$  and the other with a range of  $1918.0\text{--}1923.0 \text{ cm}^{-1}$ . The threshold current of each laser is  $\sim 300 \text{ mA}$  and the maximum

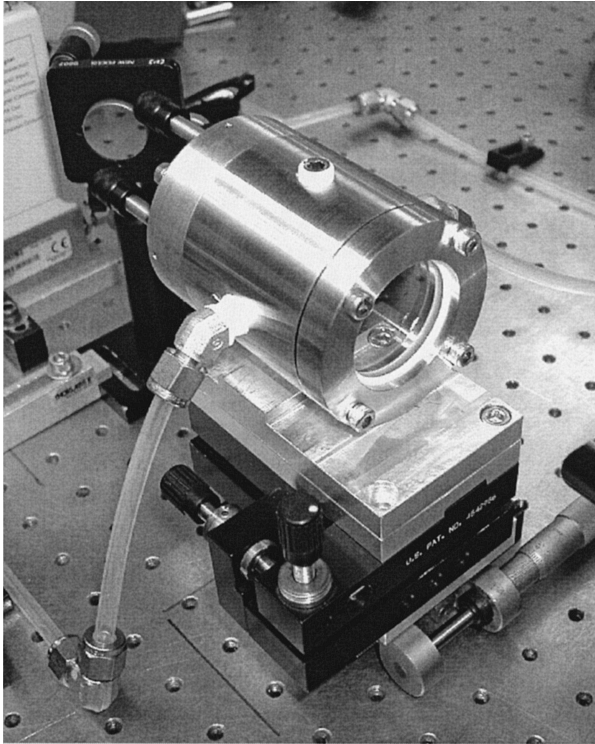


Fig. 4. Photograph of a compact OA-ICOS gas cell.

output power varies from 18 to 25 mW (depending on the wavelength and the laser).

The QC laser radiation was collimated with two positive lenses (see Fig. 3). The first lens,  $L_1$ , is an aspheric ZnSe lens with an effective focal length of 25.4 mm, a diameter of 27.94 mm, and broadband antireflection coatings (3–12  $\mu\text{m}$ ). The second lens,  $L_2$ , is a  $\text{CaF}_2$  biconvex lens with a diameter of 12.7 mm and an effective focal length of 13 mm. The collimator length is 130 mm, and the distance between the QC laser output facet and  $L_1$  is 18 mm. Approximately 80% of the emitted power is collected, assuming a divergence of  $60^\circ$  and a Gaussian beam envelope. The collimated beam diameter is approximately 3 mm and can be made divergent or convergent by changing the position of  $L_2$  relative to  $L_1$ . This degree of freedom is important for optimal laser-cavity-mode coupling. Another advantage of the collimator is that, by its use, a simple routine to perform optical alignment and realignment for different QC lasers on the same chip is possible. A He-Ne laser is used for coarse alignment because the 5.2- $\mu\text{m}$  radiation is not visible. The final alignment of collimating lenses was performed with an IR camera (ThermoVision).

The laser beam exiting the collimator is directed to the compact OA-ICOS cavity described in Section 2 (also see Fig. 4). For spectroscopic measurements, laser radiation is scanned over a specific spectral range containing the gas absorption features of interest. Laser radiation is coupled into the cavity via the accidental coincidence of the laser frequency with a cavity mode.

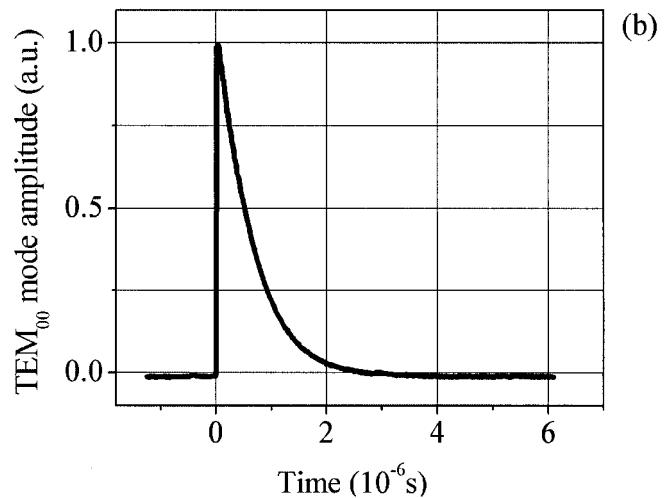
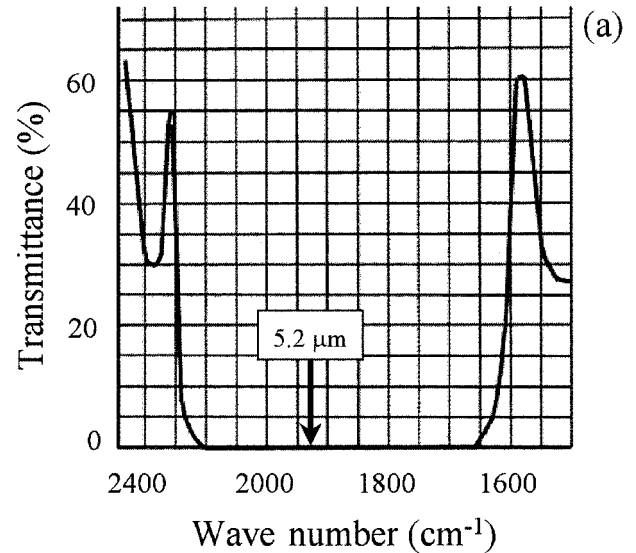


Fig. 5. (a) Spectral characteristic of a mid-IR high-reflectivity mirror (diameter of 50.8 mm, ROC of 1 m; data provided by Los Gatos Research, Inc., Mountain View, Calif.). (b) Typical ring-down event of 0.7  $\mu\text{s}$ .

The radiation exiting the cell is focused onto a  $\text{LN}_2$ -cooled photovoltaic HgCdTe detector (1- $\text{mm}^2$  sensitive area) with a built-in  $10^4$  V/A transimpedance preamplifier (Model KMPV8-1-J1/DC, Kolmar Technologies, Newburyport, Mass.). An off-axis parabolic mirror (3-in. diameter, 3-in focal length; 1 in = 25.4 mm) is used to collect the transmitted cavity output, which was focused onto the detector area, thereby maximizing the light signal. A personal computer with a data acquisition and processing system based on LabVIEW 6.1 software is used for data accumulation, storage, and time averaging. Averaging many laser frequency scans results in smoothing of the cavity resonance spikes.

The transmission of the cavity mirrors as a function of frequency is depicted in Fig. 5(a). The reflec-

tion coefficient or mirror losses at a specific wavelength can be estimated from the cavity decay time of the TEM<sub>00</sub> mode, assuming that the reflectivity is uniform across the entire mirror surface.<sup>29</sup> The intensity of a light pulse, trapped in an optical resonator, decreases exponentially with a time constant determined by the cavity finesse. In the case of a stable evacuated cavity formed by two identical mirrors and negligible Mie and Rayleigh scattering losses, the decay time  $\tau_{\text{empty}}$  for the TEM<sub>00</sub> cavity mode or cavity ringdown time is defined only by the cavity length and the reflection coefficient ( $R$ ) of the mirrors:

$$\tau_{\text{empty}} = \frac{L}{c} \frac{1}{(1 - R)}, \quad (5)$$

where  $L$  is the cavity length (5.3 cm) and  $c$  is the speed of light. For Eq. (5) we should consider the maximum experimental value of the decay time because the TEM<sub>00</sub> mode has the lowest diffraction losses and thus the maximum ring down time. We measured  $\tau_{\text{empty}} = 0.7 \mu\text{s}$ ; thus,  $R \approx 99.975\%$  or 250 ppm in terms of mirror losses. A ring down event with a typical decay time is shown in Fig. 5(b). The QC laser linewidth has been estimated as described by Kosterev *et al.*<sup>21</sup> From the cavity transmission resonance spikes, we obtain 2.9 and 3.5 MHz for the linewidths of the two cw QC lasers used in this work.

The principal limitation to the detection sensitivity of ICOS is the cavity-mode noise that results from incomplete averaging of the optical-cavity transmission [see Fig. 2(b)]. This problem becomes more pronounced in the case of a short optical cavity. This can be explained by the larger FSR and hence the wider gaps between the cavity transmission peaks, as well as by the higher mechanical stability of the short cavity. Our observations have shown that even for off-axis beam alignment, natural cavity instabilities, such as acoustic noise and temperature variations, are not sufficient to average out the cavity-mode structure. Therefore, in addition to laser scanning, the length of the cavity is dithered by PZT actuators at 200 Hz. The PZT mirror displacement amplitude corresponds to  $>7$  FSR of the modes that result from off-axis alignment and therefore is sufficient to wash out the throughput spikes. The absorption signal is extracted from a measurement of the time-integrated light intensity that leaks out of the cavity.

A gas-flow system enables us to control flow rate and perform NO concentration measurements at reduced pressures (to eliminate line broadening and minimize interference by other gases) and known flow conditions. A pressure controller can provide gas-cell pressures ranging from 1 to 100 Torr. The gas-flow system is also configured to permit off-line NO measurements of breath samples collected in special medical breath bags (Model QT00830-P, Quintron, Milwaukee, Wisc.).

The reference channel of the gas analyzer system consists of a 10-cm-long cell filled with 1 Torr of pure NO and a room-temperature photodetector with a

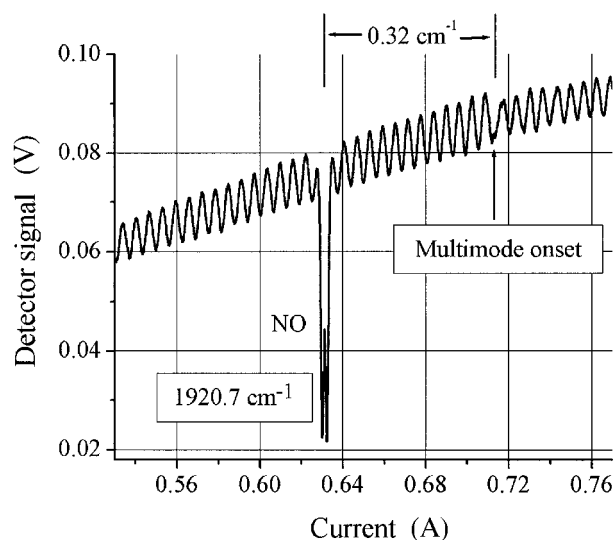


Fig. 6. Spectral calibration of the QC laser scan using an air-spaced Fabry-Perot etalon (separation of reflecting surfaces is 20 cm; FSR = 0.025 cm<sup>-1</sup>).

preamplifier (Model PDI-10.6, Boston Electronics Corp., Brookline, Mass.). The laser scan is frequency calibrated by use of an air-spaced Fabry-Perot etalon that consists of two 30' wedged ZnSe windows ( $W_1$  and  $W_2$ ) separated by 20 cm and that is temporarily inserted in the reference channel laser beam path. The FSR of this etalon is 0.025 cm<sup>-1</sup> with a fringe contrast of  $\sim 8\%$ , which is sufficient to perform a frequency calibration of the acquired NO spectra. A portion of this calibration data is depicted in Fig. 6. The onset of multimode lasing at a current of  $\sim 0.71$  A is apparent. All QC laser based NO concentration measurements were performed in single-frequency laser operation.

#### 4. Mid-IR NO Detection

According to the HITRAN database,<sup>30</sup> the fundamental absorption band for NO is located in the region from 1780 to 1950 cm<sup>-1</sup>. The optimum NO target wavelength is 1900.08 cm<sup>-1</sup> for the  $R(6.5)$  transition when the maximum line intensity and minimum interference from nearby absorption lines from other trace-gas species are taken into account.<sup>31</sup> The intensity of the  $R(6.5)$  line is  $S = 6.0 \times 10^{-20}$  cm<sup>-1</sup>/(molecule cm<sup>-2</sup>). However, the two available QC lasers cover the spectral ranges 1918.0 – 1923.0 cm<sup>-1</sup> (QC laser 1) and 1911.5 – 1917.5 cm<sup>-1</sup> (QC laser 2), which do not overlap the optimum NO line at 1900.08 cm<sup>-1</sup>. Therefore a different choice of target wavelength was required.

Figure 7 depicts a HITRAN-based simulation of a H<sub>2</sub>O-CO<sub>2</sub>-NO mixture absorption spectrum in ambient air in the range covered by QC lasers 1 and 2. The total pressure is 50 Torr and the optical path length is  $\sim 100$  m (typical value for our compact ICOS cavity). The H<sub>2</sub>O and CO<sub>2</sub> concentrations correspond to levels present in human breath. Only NO lines that do not suffer from H<sub>2</sub>O and CO<sub>2</sub> interfer-

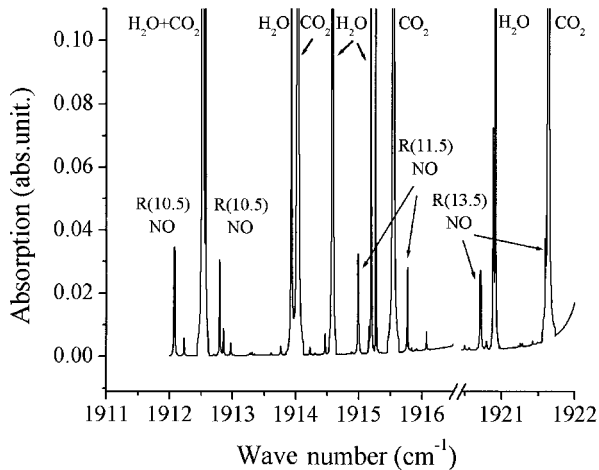


Fig. 7. HITRAN-based simulation of mid-IR absorption spectrum of a NO-CO<sub>2</sub>-H<sub>2</sub>O mixture in the tuning range of the two available QC lasers. The total pressure of the mixture is 50 Torr; path length is 100 m; concentrations of NO, CO<sub>2</sub>, and H<sub>2</sub>O are 0.5 ppbv, 4%, and 1%, respectively.

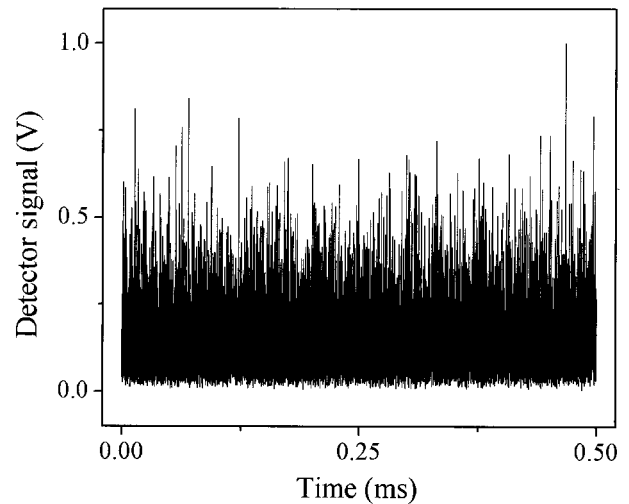


Fig. 8. Typical transmitted intensity through the OA-ICOS cavity for a single laser current scan. The QC laser scan frequency is 2 KHz.

ence are presented. The HITRAN 92 database was used instead of the more recent 96 and 2000 versions because of an absence of the NO pressure-broadening coefficient in the two more recent editions. The NO absorption lines  $R(10.5)$  at  $1912.7 \text{ cm}^{-1}$ ,  $R(11.5)$  at  $1915.0 \text{ cm}^{-1}$ , and  $R(13.5)$  at  $1920.7 \text{ cm}^{-1}$  are suitable for breath analysis. Moreover, the QC-laser tuning range covers several CO<sub>2</sub> lines, which can be used for internal calibration in breath analysis. The strongest NO line accessible with QC laser 2 is  $R(10.5)$  with a line intensity of  $S = 5.17 \times 10^{-20} \text{ cm}^{-1}/(\text{molecule cm}^{-2})$ .

### 5. Experimental Results

As described in Section 2, the off-axis laser beam cavity alignment decreases the cavity FSR and excites a large number of transverse cavity modes. The typical transmitted intensity through the cavity for off-axis alignment for a single laser current scan is depicted in Fig. 8. The high number of excited cavity modes permits such cw laser radiation-cavity interaction to be considered as noncoherent on average. The cavity serves as a simple multipass cell with a total optical path  $P$ , which depends on the reflectivity and the distance between the mirrors. According to Ref. 17, the laser power transmitted through the cavity is

$$I = I_0 C_p \frac{(1 - R)^2}{2[(1 - R) + kL]}, \quad (6)$$

where  $I_0$  is the initial laser power,  $C_p$  is a spatial coupling parameter (between 0 and 1), and  $k$  is the absorption coefficient. For weak absorption and for perfect laser-cavity mode coupling ( $C_p = 1$ ), Eq. (6) can be rewritten as

$$\frac{I}{I_0} \approx \frac{1 - R}{2} \left( 1 - \frac{kL}{1 - R} \right), \quad (7)$$

where it is assumed that  $kL \ll (1 - R)$ .  $P = L/(1 - R)$  is the theoretical optical path length from Eq. (7).

For a cavity without absorption, the optical throughput is equal to  $(1 - R)/2$  [ $(1 - R)/2 \ll 1$ , because  $R \sim 1$ ]. This explains the need for a sensitive photodetector for this technique. Equation (6) is the basis for quantitative measurements that use the ICOS approach. Once the cavity alignment is accomplished, a calibration procedure must be performed to estimate the effective optical path length  $P_{\text{eff}} < P$ . The effective optical path length for a particular cavity alignment should be substituted for the theoretical path length  $P$  given above. For a particular configuration  $P_{\text{eff}}$  can be written in the form

$$P_{\text{eff}} = \frac{L}{1 - R_{\text{eff}}}, \quad (8)$$

where  $R_{\text{eff}}$  is the effective mirror reflectivity and is less than the value of  $R$  measured for the TEM<sub>00</sub> mode.

For ICOS path-length calibration we followed the method described in Ref. 19 that measures the change of cavity transmission caused by a known concentration of an absorbing gas, such as a CO<sub>2</sub>. CO<sub>2</sub> has a weak absorption line at  $1921.66 \text{ cm}^{-1}$ . The cavity transmission  $T$  (absorption  $A = 1 - T$ ) was measured at the center of the CO<sub>2</sub> absorption line for different concentration levels, starting with pure CO<sub>2</sub>. The total pressure was always set to 100 Torr. According to Ref. 19 the absorption of the cavity can be given by

$$A = \frac{kL}{(1 - R_{\text{eff}}) + kL}. \quad (9)$$

Experimental results, together with the fitting curve based on Eq. (9), are shown in Fig. 9. It was found from fitting parameters that the effective path length for this condition and particular cavity align-

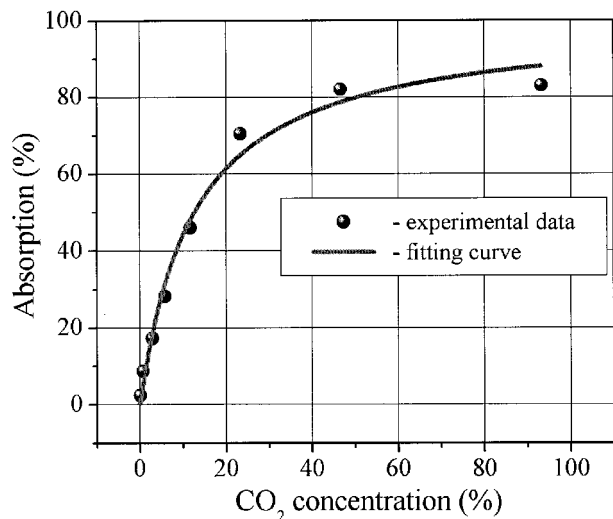


Fig. 9. OA-ICOS absorption ( $1 - I/I_0$ ) as a function of  $\text{CO}_2$  concentration in a  $\text{CO}_2$ -air mixture. Curve fitting parameters yield the effective optical path length of 80 m for a specific OA-ICOS cavity alignment.

ment is 80 m. This is compared with the value obtained from the cavity ringdown time of 106 m ( $P_{\text{eff}} = (c/2)\tau$ , where the division by 2 is explained in Ref. 24). Considering that the reflectivity is unlikely to be constant across the mirror surfaces and that  $\tau$  is uncertain, this is satisfactory agreement. This evaluation for  $P_{\text{eff}}$  was confirmed by comparing the measured amplitude for a NO absorption line with the known concentration from a calibration mixture with the HITRAN simulation for the same line and concentration. This estimate yielded an effective path length of 75 m, which corresponds to  $\sim 1,400$  passes of the laser beam inside the cavity.

The OA-ICOS technique was tested by use of two calibration mixtures of NO in  $\text{N}_2$  (Scott Specialty Gases, Inc., Plumsteadville, Pa.) with known NO concentrations of 490 and 94.9 ppbv, respectively, at a pressure of 100 Torr. The NO concentration for the first mixture was independently measured by use of CRDS,<sup>21</sup> and for the second calibration mixture, the NO concentration was determined by means of chemiluminescence. The time-integrated transmitted intensity of the OA-ICOS cell filled with two NO- $\text{N}_2$  calibration mixtures for  $5 \times 10^4$  averaged scans of the  $R(13.5)$  NO line at  $1920.7 \text{ cm}^{-1}$  is depicted in Fig. 10(a) after a third-order polynomial baseline correction and scan frequency calibration. The laser scan frequency was 3 kHz. The measured absorption spectra are in good agreement with the HITRAN simulation for an effective absorption path length of 75 m. An estimate of the detection sensitivity can be obtained from the deviation of the best-fit coefficients for a Voigt fit of the NO absorption line, which yields a noise-equivalent sensitivity of 10 ppbv for a  $1\sigma$  deviation of the best-fit coefficient. Experimental results, together with the fitting curve, are given in Fig. 10(b).

Feasibility experiments with OA-ICOS and wave-

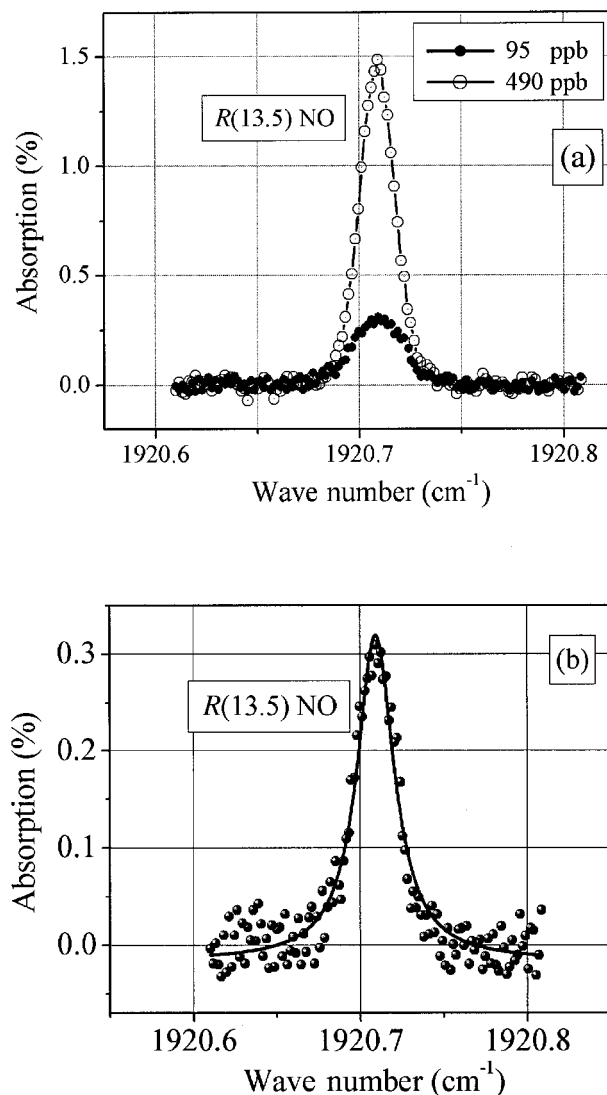


Fig. 10. (a)  $R(13.5)$  NO absorption line at  $1920.7 \text{ cm}^{-1}$  after baseline correction and frequency calibration. NO concentration measurements for two different calibration mixtures: 490-ppbv NO in  $\text{N}_2$  and 95-ppbv NO in  $\text{N}_2$ . The total gas mixture pressure is 100 Torr. (b) Voigt fit of the  $R(13.5)$  NO absorption line data (same 95-ppbv NO in  $\text{N}_2$  mixture).

length modulation spectroscopy (WMS)<sup>32</sup> were performed to determine the biogenic NO concentrations from nasal-exhaled air. The current for QC laser 2 was scanned across the NO line by use of a triangular current ramp at a frequency of 8 Hz. A sinusoidal dither of  $f \sim 5 \text{ kHz}$  (maximum for the laser current driver used in this work) was superimposed on the QC laser current ramp. The second-harmonic ( $2f$ ) signal of the OA-ICOS cavity output was sampled with a lock-in amplifier and averaged with a data acquisition card (DAQ Card 6062E, National Instruments, Austin, Tex.) and LabVIEW software. The amplitude of the  $2f$  spectra is directly proportional to the NO concentration, which can be retrieved from calibration measurements. Figure 11 depicts  $2f$  spectra of the  $R(10.5)$  NO line at  $1912.07 \text{ cm}^{-1}$  for the

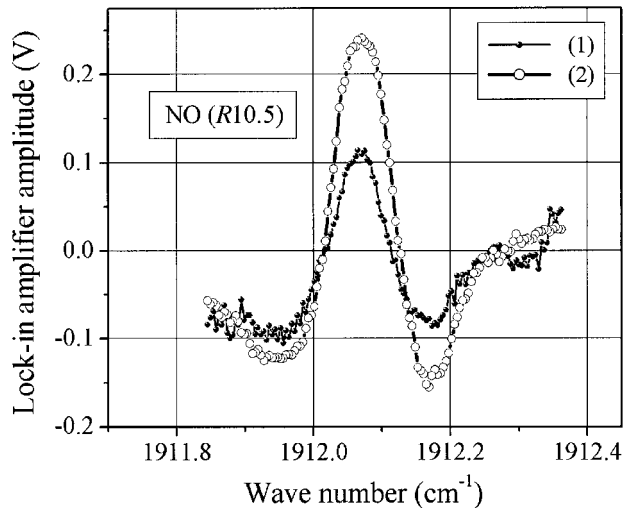


Fig. 11. NO concentration measurement with wavelength modulation applied to OA-ICOS: (1) NO concentration of 53 ppbv in nasal breath; (2) NO-N<sub>2</sub> calibration mixture for 95-ppbv NO.

95-ppbv NO:N<sub>2</sub> calibration mixture as well as for collected nasal NO. The nNO concentration was deduced to be 53 ppbv. It is apparent from these results (see Figs. 10 and 11) that wavelength modulation spectroscopy yields a better detection sensitivity than does direct absorption spectroscopy. The increase of the SNR is >5, and the noise-equivalent detection sensitivity is ~2 ppbv. The SNR could be further improved by use of a faster QCL current driver, which would enable us to achieve optimum values for the laser current ramp and sinusoidal dithering frequencies.

## 6. Summary

A cw QC laser based NO sensor that uses a compact OA-ICOS cell has been developed, and its performance characteristics have been investigated and compared with previous gas analyzer designs based on CRDS and ICOS. The OA-ICOS-based sensor offers a noise-equivalent sensitivity of 10 ppbv that is similar to that of a CRDS-based sensor platform, but it is easier to align and more robust during long-term operation. Feasibility experiments of biogenic nNO concentration measurements from the nasal cavity have been performed by adding wavelength modulation to improve the detection sensitivity. A wavelength modulation spectroscopy noise-equivalent sensitivity of 2 ppbv has been achieved. The total data acquisition and averaging time was 15 s in both cases. Although this time exceeds a typical breath-cycle duration, the time required for a single data-point measurement is much shorter (<1 s). Therefore the described NO measurement procedure can be modified to measure NO concentration as a function of breath-cycle phase. To achieve this goal, primary data should be collected during several breath cycles and later sorted and averaged separately, depending on the breath-cycle phase.

The authors thank C. Gmachl (formerly at Lucent Technologies and now with Princeton University) for her invaluable scientific and technical support; Mark Allen of Physical Sciences, Inc. (PSI) for his collaboration and financial support, provided by a NASA-National Cancer Institute grant to PSI; B. Dekker and D. Sonnenfroh of PSI for helpful comments regarding our manuscript; and Anthony O'Keefe of Los Gatos Research, Inc. for supplying the ultralow-loss cavity mirrors used in this work. The research was also partially supported by the Welch Foundation, the Texas Advanced Technology program, and the Office of Naval Research through a subaward from Texas A&M University. One of the authors (Yu. Bakhrkin) acknowledges the award of a fellowship from the Institute for Space Systems Operations, University of Houston, Texas.

## References

1. M. W. Sigrist, *Air Monitoring by Spectroscopic Techniques* (Wiley, New York, 1994).
2. D. D. Nelson, J. L. Jimenez, G. J. McRae, M. S. Zahniser, and C. E. Kolb, "Remote sensing of NO and NO<sub>2</sub> emission from heavy-duty diesel trucks using tunable diode lasers," in *Application of Tunable Diode and Other Infrared Sources for Atmospheric Studies and Industrial Processing Monitoring II*, A. Fried, ed., Proc. SPIE **3758**, 180–190 (1999).
3. W. H. Weber, T. J. Remillard, R. E. Chase, J. F. Richert, F. Capasso, C. Gmachl, A. L. Hutchinson, D. L. Sivco, J. N. Bailargeon, and A. Y. Cho, "Using a wavelength-modulation quantum cascade laser to measure NO concentration in the parts-per-billion range for vehicle emissions certification," *Appl. Spectrosc.* **56**, 706–714 (2002).
4. S. A. Kharitonov and P. J. Barnes, "Clinical aspects of exhaled nitric oxide," *Eur. Respir. J.* **16**, 781–792 (2000).
5. S. A. Kharitonov and P. J. Barnes, "Exhaled markers of pulmonary disease," *Am. J. Respir. Crit. Care Med.* **163**, 1693–1722 (2001).
6. B. Gaston, J. M. Drazen, J. Loscalzo, and J. S. Stamler, "The biology of nitrogen oxide in the airways," *Am. J. Respir. Crit. Care Med.* **149**, 538–551 (1994).
7. K. Bhagat and P. Vallance, "Nitric oxide 9 years out," *J. R. Soc. Med.* **89**, 667–673 (1996).
8. P. Murtz, L. Menzel, W. Bloch, A. Hess, O. Michel, and W. Urban, "LMR spectroscopy: a new sensitive method for on-line recording of nitric oxide in breath," *J. Appl. Physiol.* **86**, 1075–1080 (1999).
9. D. H. Yates, "Role of exhaled nitric oxide in asthma," *Immunol. Cell Biol.* **79**, 178–190 (2001).
10. L. Prieto, "Measurements of exhaled nitric oxide concentration in asthma. Technical aspects and clinical usefulness," *Allergol. Immunol. Clin.* **17**, 72–87 (2002).
11. N. Binding, W. Muller, P. A. Czeschinski, and U. Witting, "NO chemiluminescence in exhaled air: interference of compounds from endogenous or exogenous sources," *Eur. Respir. J.* **16**, 499–503 (2000).
12. H. W. Shin, C. M. Rose-Gottron, R. S. Sufi, F. Perez, D. M. Cooper, A. F. Wilson, and S. C. George, "Flow-independent nitric oxide exchange parameters in cystic fibrosis," *Am. J. Respir. Crit. Care Med.* **165**, 349–357 (2002).
13. M. Maniscalco, V. Di Mauro, E. Farinaro, L. Carratu, and M. Sofia, "Transient decrease of exhaled nitric oxide after acute exposure to passive smoke in healthy subjects," *Arch. Environ. Health* **57**, 437–440 (2002).
14. G. Litfin, C. R. Pollock, R. F. Curl, Jr., and F. K. Tittel, "Sen-

- sitivity enhancement of laser absorption spectroscopy by magnetic rotation effect," *J. Chem. Phys.* **12**, 6602–6605 (1980).
15. H. Ganser, W. Urban, and J. M. Brown, "The sensitive detection of NO by Faraday modulation spectroscopy with a quantum cascade laser," *Mol. Phys.* **101**, 545–550 (2003).
  16. C. Roller, K. Namjou, J. D. Jeffers, M. Camp, A. Mock, P. J. McCann, and J. Grego, "Nitric oxide breath testing by tunable-diode laser absorption spectroscopy: application in monitoring respiratory inflammation," *Appl. Opt.* **41**, 6018–6029 (2002).
  17. A. A. Kosterev and F. K. Tittel, "Chemical sensors based on quantum cascade lasers," *IEEE J. Quantum Electron.* **38**, 582–591 (2002).
  18. E. V. Stepanov, P. V. Zyrianov, and V. A. Miliavev, "Single-breath detection with tunable diode lasers for pulmonary disease diagnosis," in *ALT'98 Selected Papers on Novel Laser Methods in Medicine and Biology*, A. M. Prokhorov, V. I. Pustovoy, and G. P. Kuz'min, eds., *Proc. SPIE* **3829**, 103–109 (1999).
  19. L. Menzel, A. A. Kosterev, R. F. Curl, F. K. Tittel, C. Gmachl, F. Capasso, D. L. Sivco, N. J. Baillargeon, A. L. Hutchinson, A. Y. Cho, and W. Urban, "Spectroscopic detection of biological NO with a quantum cascade laser," *Appl. Phys. B* **72**, 859–863 (2001).
  20. D. D. Nelson, J. H. Shorter, J. B. McManus, and M. S. Zahniser, "Sub-part-per-billion detection of nitric oxide in air using a thermoelectrically cooled mid-infrared quantum cascade laser spectrometer," *Appl. Phys. B* **75**, 343–350 (2002).
  21. A. A. Kosterev, A. L. Malinovsky, F. K. Tittel, C. Gmachl, F. Capasso, D. L. Sivco, J. N. Baillargeon, A. L. Hutchinson, and A. Y. Cho, "Cavity ringdown spectroscopic detection of nitric oxide with continuous-wave quantum-cascade laser," *Appl. Opt.* **40**, 5522–5529 (2001).
  22. A. O'Keefe, "Integrated cavity output analysis of ultra-weak absorption," *Chem. Phys. Lett.* **293**, 331–336 (1998).
  23. R. Englen, G. Berden, R. Peeters, and G. Meijer, "Cavity enhanced absorption and cavity enhanced magnetic rotation spectroscopy," *Rev. Sci. Instrum.* **69**, 3763–3769 (1998).
  24. J. B. Paul, L. Larson, and J. G. Anderson, "Ultrasensitive absorption spectroscopy with a high-finesse optical cavity and off-axis alignment," *Appl. Opt.* **40**, 4904–4910 (2001).
  25. D. S. Baer, J. B. Paul, M. Gupta, and A. O'Keefe, "Sensitive absorption measurements in near-infrared region using off-axis integrated-cavity-output spectroscopy," *Appl. Phys. B* **75**, 261–265 (2002).
  26. V. L. Kasyutich, C. E. Canosa-Mas, C. Pfrang, S. Vaughan, and R. P. Wayne, "Off-axis continuous-wave cavity-enhanced absorption spectroscopy of narrow-band and broadband absorbers using red diode lasers," *Appl. Phys. B* **75**, 755–761 (2002).
  27. D. R. Herriott, H. Kogelnik, and R. Kompfner, "Off-axis paths in spherical mirror interferometers," *Appl. Opt.* **3**, 523–526 (1964).
  28. F. Capasso, C. Gmachl, R. Paiella, A. Tredicucci, A. L. Hutchinson, D. L. Sivco, J. N. Baillargeon, and A. Y. Cho, "New frontiers in quantum cascade lasers and applications," *IEEE Sel. Top. Quantum Electron.* **6**, 931–947 (2000).
  29. J. M. Herbelin, J. A. McKay, M. A. Kwok, R. H. Ueunten, D. S. Urevig, D. J. Spenser, and D. J. Benard, "Sensitive measurement of photon lifetime and true reflectances in an optical cavity by a phase-shift method," *Appl. Opt.* **19**, 144–147 (1980).
  30. L. S. Rothman, A. Barbe, D. C. Benner, L. R. Brown, C. Camy-Peyret, M. R. Carleer, K. Chance, C. Clerbaux, V. Dana, V. M. Devi, A. Fayt, J. M. Flaud, R. R. Gamache, A. Goldman, D. Jacquemart, K. W. Jucks, W. J. Lafferty, J. Y. Mandin, S. T. Massie, V. Nemtchinov, D. A. Newnham, A. Perrin, C. P. Rinsland, J. Schroeder, K. M. Smith, M. A. H. Smith, K. Tang, R. A. Toth, J. Vander Auwera, P. Varanasi, and K. Yoshino, "The HITRAN molecular spectroscopic database: edition of 2000 including updates through 2001," *J. Quant. Spectrosc. Radiat. Transfer* **82**, 5–44 (2003).
  31. S. D. Wehe, D. M. Sonnenfroh, M. G. Allen, C. Gmachl, and F. Capasso, "Quantum-cascade laser-based sensor for CO and NO measurements in combustor exhaust flows," presented at AIAA 2001-3317, 37 Joint Propulsion Conference and Exhibit, Salt Lake City, Utah, July 8–11, 2001.
  32. D. S. Bomse, A. C. Statlon, and J. A. Silver, "Frequency modulation and wavelength modulation spectroscopies: comparison of external methods using a lead-salt diode laser," *Appl. Opt.* **31**, 718–731 (1992).